Erbium-implanted high-Q silica toroidal microcavity laser on a silicon chip

Bumki Min, Tobias J. Kippenberg, Lan Yang, and Kerry J. Vahala

Thomas J. Watson Laboratory of Applied Physics, California Institute of Technology, Pasadena, California 91125, USA

Jeroen Kalkman and Albert Polman

FOM Institute for Atomic and Molecular Physics, Kruislaan 407, 1098 SJ Amsterdam, The Netherlands

Lasing from an erbium-doped high-Q silica toroidal microcavity coupled to a tapered optical fiber is demonstrated and analyzed. Average erbium ion concentrations were in the range 0.009–0.09 at. %, and a threshold power as low as 4.5 μW and an output lasing power as high as 39.4 μW are obtained from toroidal cavities with major diameters in the range 25–80 μm. Controlling lasing wavelength in a discrete way at each whispering-gallery mode was possible by changing the cavity loading, i.e., the distance between the tapered optical fiber and the microcavity. Analytic formulas predicting threshold power and differential slope efficiency are derived and their dependence on cavity loading, erbium ion concentration, and Q factor is analyzed. It is shown that the experimental results are in good agreement with the derived formulas.

I. INTRODUCTION

Ultrahigh-quality-factor ($Q > 10^8$), dielectric microcavity resonators possessing whispering-gallery modes (WGMs) have been investigated intensively for the last decade. Cavity quality factors (Q factors) as high as 8×10^9 [1,2], along with small mode volumes, have been essential driving forces for fundamental research areas such as cavity quantum electrodynamics, nonlinear optics, biosensing, and microscale lasers [1–17]. The first studied ultrahigh-Q optical microcavities were liquid microdroplets. In the pioneering work of Chang and Campillo, nonlinear optical effects were investigated in such structures illuminated by free-space beams [3–6]. However, microdroplets are inherently transient and the free-space excitation of resonances was inefficient.

Two kinds of "solid" microcavities, which are capable of achieving ultrahigh-Q performance, have been developed to overcome these stability and efficiency issues related to liquid droplets. The older of these is a spherical "droplet" of silica which exhibits Q factors of up to 8×10^9 in the near infrared [1,2]. These solid microspheres, like their liquid counterparts, rely upon surface tension to create an exquisitely smooth dielectric boundary [2] along which the whispering-gallery modes are confined. More recently, a surface-tension-induced structure in the form of a toroidal microcavity has enabled access to Q factors in excess of 10^8, the highest value reported on a planar substrate [18]. These toroidal microcavities are silica based and fabricated on silicon chips combining standard silicon technology with ultrahigh-Q fabrication techniques. This synergistic approach allows creation of dense arrays of ultrahigh-Q microcavity structures in parallel on a silicon wafer, allowing the integration with complementary electrical, optical, or mechanical functionality. In addition, lithographic methods can be used to control size, rendering the devices highly reproducible.

Among the practical applications of ultrahigh-Q microresonators, rare-earth doped microcavity lasers have been successfully demonstrated in recent years. These include whispering-gallery-type microsphere lasers doped with neodymium, erbium, and ytterbium-sensitized erbium [8–15]. For the case of a neodymium-doped microsphere laser demonstrated by Sandoghdar *et al.* [8], the (absorbed) threshold power was as low as 200 nW. Using the chip-based toroidal microcavities described above, a sol-gel coating technique was applied recently to fabricate erbium-doped toroidal microcavity lasers on a silicon chip [16]. In addition to the advantages in fabrication, these devices provide improved spectral performance as compared to microspheres owing to their reduced modal spectra [16,18]. In particular, single-mode operation was possible in these devices. As a complementary method of gain functionalization that is more compatible with standard VLSI processing, we have recently demonstrated erbium-implantation-based toroidal microcavity lasers [17]. For both types of erbium-doped resonators (made by sol-gel processing or implantation), the internal dynamics and the dependence on cavity loading between the waveguide (tapered optical fiber) and the microcavity have not been thoroughly investigated.

In this paper, we used the ion implantation method to incorporate erbium ions into ultrahigh-Q toroidal microcavities and study in detail various lasing characteristics when these devices are coupled to a tapered optical fiber for excitation. In addition, experimental results are correlated with modeling of devices to understand the limits of performance as well as the basic lasing mechanisms. Using samples of varying sizes and erbium ion concentrations, the minimum threshold power was shown to be as low as 4.5 μW and the highest output power was measured to be 39.4 μW. A maximum unidirectional slope efficiency of 5.5% was observed. Lasing wavelength control between adjacent whispering-gallery modes was demonstrated and explained by a cavity-loading-induced change in the upper-state population of erbium ions.

The remainder of this paper is organized as follows. In Sec. II, we present a detailed description of erbium-doped high-Q toroidal microcavity lasers using coupled-mode formalism. In Sec. III, we briefly illustrate the fabrication pro-
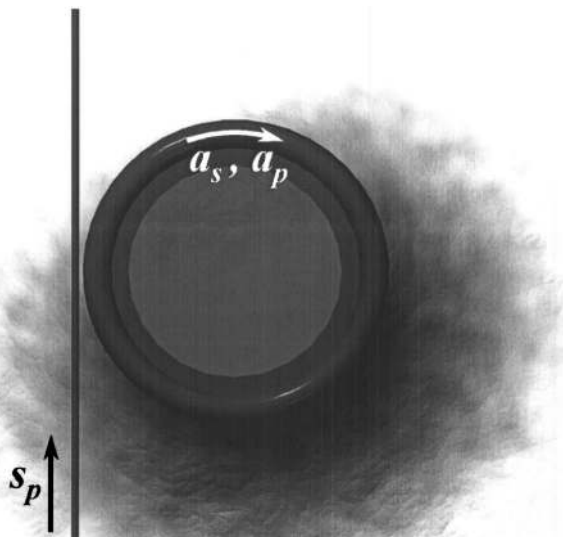
FIG. 1. Graphical rendering of the toroidal microcavity-tapered optical fiber system. Input/output waveguide (tapered optical fiber) and erbium-doped toroidal microcavity are shown along with an input pump wave s_p and internal cavity fields a_p and a_s.

cess used to create the erbium-implanted toroidal microcavities. In Sec. IV, we investigate experimentally the performance of erbium-implanted toroidal microcavity lasers and compare these experimental results with the proposed analysis. Finally, in Sec. V, we conclude and discuss future research directions.

II. ANALYSIS OF ERBIUM-DOPED HIGH-Q TOROIDAL MICROCAVITY LASERS

The analysis is based on the coupled-mode formalism for the resonator coupled to an external waveguide [19–23] with the addition of gain (or loss) terms from the excited erbium ions. Considering two resonant modes at the pump and (lasing) signal wavelengths in the microcavity, along with the pump wave coupled into the resonator from the waveguide (Fig. 1 shows the graphical rendering of the toroidal microcavity-tapered fiber system), the basic coupled equations of motion for the pump and signal field can be written as follows:

$$\frac{da_s}{dt} = -\frac{1}{2\tau_s}a_s + g_s a_s, \tag{1}$$

$$\frac{da_p}{dt} = -\frac{1}{2\tau_p}a_p - l_p a_p + i\kappa_p s_p, \tag{2}$$

where a_s, a_p are internal cavity fields at the signal and pump wavelengths ($|a_{s,p}|^2$ is normalized to the energy in the cavity; and counter-rotating field coupling induced by surface inhomogeneity is not included in this analysis), τ_s, τ_p are cavity photon lifetimes at signal and pump wavelengths (which include passive cavity loss mechanisms such as surface scattering, absorption, and waveguide coupling [1,2,22] but exclude the gain/loss caused by the erbium ions), g_s, l_p are intracavity gain (or loss) coefficients depending on the mode,

κ_p is the amplitude coupling coefficient between the resonator and the waveguide pump wave (which is defined as $\sqrt{1/\tau_{\text{ext}}}$ and can be controlled by changing the gap width between the resonator and the waveguide), and s_p is the pump field amplitude in the input waveguide ($|s_p|^2$ is normalized to the pump power in the waveguide). For simplicity, we have used the slowly varying envelope approximation (SVEA). Competing effects such as cooperative upconversion of erbium ions, excited-state absorption (pump or signal), pair-induced quenching [24–26], and the inclusion of spontaneous emission are not considered here. However, these effects can easily be incorporated analytically into the above basic equations by including appropriate additional rate terms and their associated rate equations. Mode splitting due to coupling of counter-rotating waves (induced by inhomogeneity of cavity surfaces) [21,27] is not considered.

Under steady-state conditions, the time derivative terms in (1) and (2) can be set to vanish, leading to the following two equations (3) and (4). The first equation is equivalent to the well-known threshold condition (i.e., cavity gain should be equal to cavity loss) for lasing, and the second equation relates the internal cavity energy at the pump wavelength to the input pump power at the waveguide-resonator junction

$$g_s = \frac{1}{2\tau_s}, \tag{3}$$

$$|a_p|^2 = \frac{\kappa_p^2}{\left(\dfrac{1}{2\tau_p} + l_p\right)^2}|s_p|^2. \tag{4}$$

Even though these equations seem to be decoupled from each other, they are in fact coupled since the erbium upper-state population N_2 determines both g_s and l_p as shown below [Eqs. (5) and (6)]. The intracavity gain and loss coefficients, g_s and l_p, can be expressed as

$$g_s = \frac{c}{2n_s}\left[\frac{N_2}{N_T}(\alpha_s + g_s^*) - \alpha_s\right], \tag{5}$$

$$l_p = \frac{c}{2n_p}\left[-\frac{N_2}{N_T}(\alpha_p + g_p^*) + \alpha_p\right], \tag{6}$$

where c is the speed of light, n_s, n_p are the refractive indices at the signal and pump wavelengths, respectively, N_T is the average erbium ion concentration, and $\alpha_{s,p}$ and $g_{s,p}^*$ are Giles parameters [24,25,28] originally introduced for the modeling of erbium-doped fiber amplifiers and defined as

$$\alpha_{s,p} \equiv \Gamma_{s,p} N_T \sigma_{s,p}^a, \tag{7}$$

$$g_{s,p}^* \equiv \Gamma_{s,p} N_T \sigma_{s,p}^e. \tag{8}$$

In these expressions $\Gamma_{s,p}$ is an overlap factor (defined as the dimensionless spatial overlap integral between the normalized optical intensity distribution and the normalized erbium ion distribution) at signal and pump wavelengths and $\sigma_{s,p}^{a,e}$ is the absorption/emission cross section of erbium ions at signal and pump wavelengths.
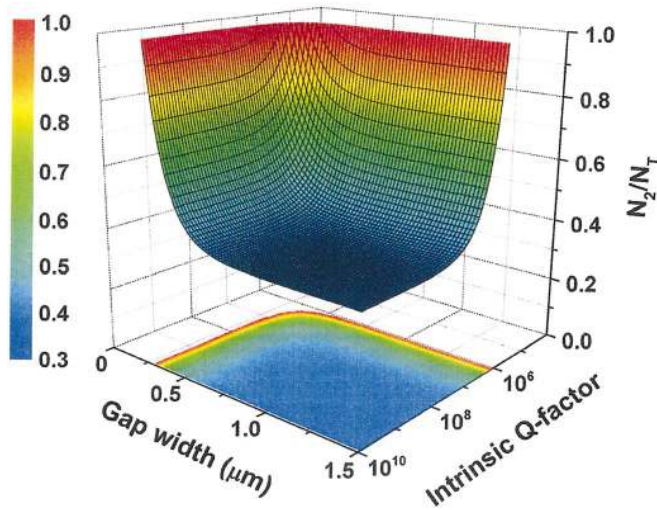
FIG. 2. (Color) Normalized upper-state population of erbium ions N_2/N_T under condition (3) calculated as a function of gap width (cavity loading) and signal intrinsic Q factor.

To fully utilize the simplicity of Giles parameters as given by (7) and (8) for further discussion, it is necessary to specify the overlap factors in the toroidal microcavities. However, to date, there has not been a detailed analytic model for the field distribution in the dielectric toroidal resonators. In addition, the erbium ion diffusion process during the laser reflow process (see Armani *et al.* [18], and also Sec. III) is not well known. Therefore, throughout this paper, the erbium ions will be assumed to diffuse homogeneously and the overlap factors of unity ($\Gamma_{s,p}=1$) for both signal and pump wavelength will be assumed for simplicity (on the assumption that the mode field distribution is well confined in the microcavity). We note that the pump wavelength used is in the range 1460–1480 nm and therefore signal and pump overlap factors will be nearly the same.

A. Upper-state population of erbium ions in microcavity

Combining Eq. (3) with (5), the normalized erbium upper-state population N_2/N_T can be expressed as follows:

$$\frac{N_2}{N_T} = \frac{\alpha_s + \alpha_s^{passive}}{\alpha_s + g_s^*}, \tag{9}$$

where the passive cavity signal loss, $\alpha_s^{passive}$, is defined as

$$\alpha_s^{passive} \equiv \frac{n_s}{c\tau_s} = \frac{2\pi n_s}{\lambda_s Q_{T,s}^{passive}}, \tag{10}$$

with $Q_{T,s}^{passive}$ the loaded quality factor at the signal wavelength, excluding the effects of erbium ions. Equation (9) is especially useful because it provides a simple relation between the normalized upper-state population in the microcavity and the parameters of microcavity and erbium ions. It reflects the well-known "clamping" of the population inversion under lasing conditions. The normalized upper-state population N_2/N_T is shown in Fig. 2 as a function of gap width (cavity loading) and signal intrinsic Q factor. The calculation is performed assuming $\Gamma_{s,p}=1$, a signal wavelength

of 1552.9 nm, erbium ion concentration of 2×10^{19} cm^{-3}, and a cavity diameter of 50 μm coupled to a phase-matched tapered fiber. In the highly undercoupled regime (large gap width between the microcavity and the tapered fiber), the normalized erbium upper-state population is determined by intrinsic signal quality factor and Giles parameters. For ultrahigh-Q factor, it is set near $\alpha_s/(\alpha_s+g_s^*)=0.39$ (determined by Giles parameters and therefore varying with lasing wavelength). At each preassumed lasing wavelength, a possible minimum N_2/N_T is defined by $\alpha_s/(\alpha_s+g_s^*)$, below which lasing will not be permitted. As the cavity loading increases (gap width decreases), the loaded signal quality factor decreases and therefore the normalized erbium upper-state population increases (favoring the possibility of shorter wavelength lasing). It is well known that the peak gain wavelength [29] and the corresponding lasing wavelength are determined by the normalized erbium upper-state population. In Sec. IV, lasing wavelength control by change of cavity loading will be further examined on the basis of Eq. (9).

B. Q factors at pump and signal wavelengths

In Eq. (9) for the population inversion, cavity loss $\alpha_s^{passive}$ at the signal wavelength is the only variable that can be controlled (after fabrication) by changing the waveguide loading of the cavity. This passive cavity signal loss $\alpha_s^{passive}$ can be expressed using the loaded Q factor as in (10). In the case of weak coupling between the resonator and the waveguide, the decomposition of the loaded Q factor for the passive (i.e., without the effects of erbium ions) microcavity is given by the following simple form:

$$\frac{1}{Q_T^{passive}} = \frac{1}{Q_o^{passive}} + \frac{1}{Q_{ext}}, \tag{11}$$

where Q_{ext} is the external Q factor of the microcavity (determined by cavity loading) and $Q_o^{passive}$ is the intrinsic Q factor originating from loss mechanisms such as cavity surface scattering, adsorbed surface water, residual OH$^-$ impurities, whispering-gallery leakage, and bulk material absorption loss [1,2]. For undoped silica microcavities having diameters larger than approximately 20 μm and for the wavelength band of interest in this work (1400–1600 nm), intrinsic Q factors are limited primarily by water adsorption and surface scattering [2,30]. It should also be noted that in the present work, the erbium implantation process could potentially alter $Q_o^{passive}$ by the introduction of absorbing (point) defects in the ion beam modified silica network structure [31].

Transitions between the ground- and excited-state manifolds ($^4I_{15/2}$ and $^4I_{13/2}$) of erbium introduce signal gain and pump absorption terms as described in (1) and (2). By extending the definition of Q factor to include these effects, the following "erbium-population-inversion dependent" cavity Q factors can be obtained:

$$\frac{1}{Q_s^{Er}} = \frac{\lambda_s}{2\pi n_s}\left[-\frac{N_2}{N_T}(\alpha_s+g_s^*)+\alpha_s\right] = -\frac{\lambda_s\alpha_s^{passive}}{2\pi n_s} = -\frac{1}{Q_{T,s}^{passive}}, \tag{12}$$

$$\frac{1}{Q_p^{Er}} = \frac{\lambda_p}{2\pi n_p}\left[-\frac{N_2}{N_T}(\alpha_p + g_p^*) + \alpha_p\right] = \frac{\lambda_p}{2\pi n_p}\left[-\frac{\alpha_p + g_p^*}{\alpha_s + g_s^*}(\alpha_s\right.$$

$$\left. + \alpha_s^{passive}) + \alpha_p\right] = \frac{\lambda_p}{2\pi n_p}\left(\frac{g_s^*\alpha_p - g_p^*\alpha_s}{\alpha_s + g_s^*}\right)$$

$$- \frac{n_s\lambda_p}{n_p\lambda_s}\frac{\alpha_p + g_p^*}{\alpha_s + g_s^*}\frac{1}{Q_{T,s}^{passive}}, \tag{13}$$

where Eq. (9) has been used to relate the population inversion to other parameters. Using these intuitive definitions, the total Q factors (including the effects of gain/loss from excited erbium ions) for the signal (lasing mode) and pump wave can be expressed as follows:

$$\frac{1}{Q_{T,s}} = \frac{1}{Q_s^{Er}} + \frac{1}{Q_{T,s}^{passive}} = 0, \tag{14}$$

$$\frac{1}{Q_{T,p}} = \frac{1}{Q_p^{Er}} + \frac{1}{Q_{T,p}^{passive}} = \frac{\lambda_p}{2\pi n_p}\left(\frac{g_s^*\alpha_p - g_p^*\alpha_s}{\alpha_s + g_s^*}\right)$$

$$- \frac{n_s\lambda_p}{n_p\lambda_s}\frac{\alpha_p + g_p^*}{\alpha_s + g_s^*}\frac{1}{Q_{T,s}^{passive}} + \frac{1}{Q_{T,p}^{passive}} = \frac{1}{Q_{o,p}^{Er}} + \frac{1}{Q_{ext,p}}. \tag{15}$$

The condition stated in Eq. (14), which is the threshold condition expressed in terms of Q factor, suggests that an infinite Q factor for the signal wave is possible (i.e., perfect balance of gain and loss). However, the infinite Q factor is a by-product of neglecting spontaneous emission in Eq. (1). In reality, this will not be observed because of the spontaneous emission, which is also responsible for a finite laser linewidth.

Beside the form of Eq. (14) and (15) in lasing operation, another interesting regime is the condition of negligible upper-state population inversion (i.e., weak pump condition). The weakly pumped intrinsic Q factors (including absorption both in the pump and the emission band) are given by setting the population inversion N_2/N_T to zero in (12) and (13)

$$Q_{wp,s}^{Er} \approx \frac{2\pi n_s}{\alpha_s\lambda_s} = \frac{2\pi n_s}{\Gamma_s N_T \sigma_s^a \lambda_s}, \tag{16}$$

$$Q_{wp,p}^{Er} \approx \frac{2\pi n_p}{\alpha_p\lambda_p} = \frac{2\pi n_p}{\Gamma_p N_T \sigma_p^a \lambda_p}. \tag{17}$$

Here, a "*wp*" subscript denotes that these Q factors correspond to the weakly pumped case (i.e., negligible upper-state population). Clearly, in the weak pump condition, higher erbium concentrations will reduce these quantities and, in turn, lower the total cavity Q factor. These weakly pumped intrinsic Q factors are easily measured in experiments. Their measurement, along with knowledge of basic parameters, gives a rough estimate of the erbium concentration and overlap factor.

C. Lasing output power

To obtain the output lasing power as a function of input pump power, the upper-state population is first expressed in

terms of the internal cavity fields. From the rate equation for an excited population of erbium ions under steady-state conditions [24,25,28], the following expression results:

$$\frac{N_2}{N_T} = \frac{\dfrac{\alpha_s}{\nu_s}\dfrac{|a_s|^2}{n_s V_m^s} + \dfrac{\alpha_p}{\nu_p}\dfrac{|a_p|^2}{n_p V_m^p}}{\dfrac{\alpha_s + g_s^*}{\nu_s}\dfrac{|a_s|^2}{n_s V_m^s} + \dfrac{\alpha_p + g_p^*}{\nu_p}\dfrac{|a_p|^2}{n_p V_m^p} + \dfrac{hN_T}{c\tau_{Er,N_T}}}, \tag{18}$$

where $V_m^{s,p}$ are the effective pump and signal mode volumes in the microcavity, h is the Planck's constant, and τ_{Er,N_T} is the lifetime of the erbium ions.

This normalized upper-state population is equated to its threshold value (assuming lasing condition and population clamping) from Eq. (9). After simple algebraic manipulation, the following relation between internal circulating pump and signal energies can be obtained:

$$|a_s|^2 = \left(\frac{\nu_s n_s V_m^s}{\nu_p n_p V_m^p}\right)\frac{\alpha_p(\alpha_s + g_s^*) - (\alpha_p + g_p^*)(\alpha_s + \alpha_s^{passive})}{\alpha_s^{passive}(\alpha_s + g_s^*)}|a_p|^2$$

$$- N_T h\nu_s V_m^s \frac{\alpha_{Er}(\alpha_s + \alpha_s^{passive})}{\alpha_s^{passive}(\alpha_s + g_s^*)}, \tag{19}$$

where $\alpha_{Er} \equiv n_s/c\tau_{Er,N_T}$. To relate these internal field quantities to the fiber-taper coupled quantities, the internal pump energy $|a_p|^2$ is related to the input waveguide power $|s_p|^2$ through the following expression [obtained by combining (4), (6), and (9)]:

$$|a_p|^2$$

$$= \frac{4n_p^2\kappa_p^2(\alpha_s + g_s^*)^2}{c^2[(\alpha_p + \alpha_p^{passive})(\alpha_s + g_s^*) - (\alpha_p + g_p^*)(\alpha_s + \alpha_s^{passive})]^2}$$

$$\times |s_p|^2. \tag{20}$$

Expressions (19) and (20) account for both waveguide loading and population-dependent coupling effects. To convert from internal cavity energy to output lasing power, the internal energy expression (19) is multiplied by κ_s^2 ($P_L = \kappa_s^2 \times |a_s|^2$).

Figure 3 shows the output lasing power as a function of input pump power for different cavity loading conditions. Input parameters are the same as for the calculations in Fig. 2. In addition, a pump wavelength of 1471 nm and $Q_o^{passive} = 4 \times 10^7$ are used. As can be seen, the lasing threshold is a sensitive function of the gap width. The slope efficiency, defined as the differential output power versus input power, is also strongly dependent on the coupling conditions. In the next section, we will further discuss the threshold power and differential slope efficiency.

D. Threshold and slope efficiency

The input (fiber-launched) threshold pump power can be obtained directly from Eqs. (19) and (20) by setting the internal circulating signal energy to zero and solving for the required pump power
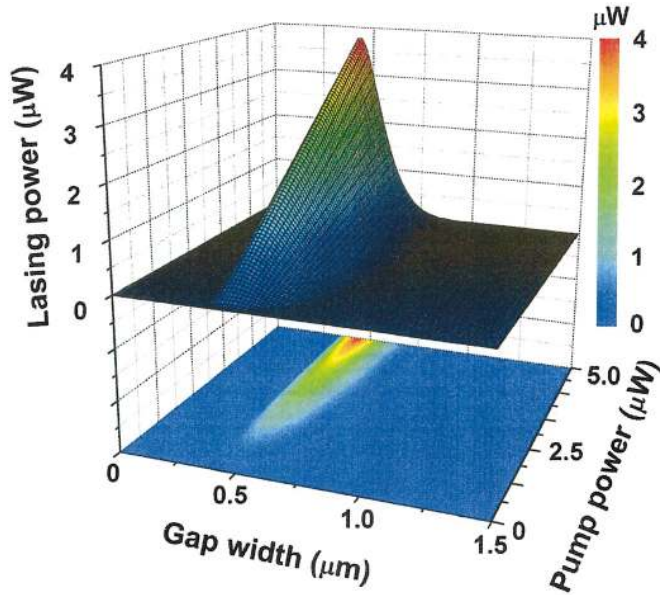
FIG. 3. (Color) Lasing power calculated as a function of input pump power and gap width.

$$|s|_{th}^2 = N_T h \nu_s V_m^s \left(\frac{\nu_s n_s V_m^s}{\nu_p n_p V_m^p} \right) \left(\frac{c^2}{4 n_p^2 \kappa_p^2} \right)$$

$$\times \frac{[(\alpha_p + \alpha_p^{passive})(\alpha_s + g_s^*) - (\alpha_p + g_p^*)(\alpha_s + \alpha_s^{passive})]^2}{(\alpha_s + g_s^*)^2}$$

$$\times \frac{\alpha_{Er}(\alpha_s + \alpha_s^{passive})}{\alpha_p(\alpha_s + g_s^*) - (\alpha_p + g_p^*)(\alpha_s + \alpha_s^{passive})}. \quad (21)$$

It should be noted that the threshold power derived here is a lower limit, as modal coupling of counter-rotating pump waves [21,27], concentration-related quenching, and excited state absorption are not taken into account.

To obtain an expression for the coupled threshold power rather than input threshold power, it is necessary to account for the power coupled from the tapered optical fiber into the cavity (assuming perfect ideality [22]). The pump transmission is given by

$$T_p = \left| -1 + i\kappa_p \frac{a_p}{s_p} \right|^2. \quad (22)$$

This quantity can be easily calculated using Eq. (20), and different cavity loading conditions can be divided into three characteristic regimes on the basis of (22). The three regimes are overcoupled ($0 < T_p < 1$, smaller gap width than critically coupled position), critically coupled ($T_p = 1$), and undercoupled condition ($0 < T_p < 1$, larger gap width than critically coupled position), respectively. The coupled threshold power can now be expressed simply as

$$P_{th}^{coupled} = (1 - T_p)|s|_{th}^2. \quad (23)$$

The differential slope efficiency expression can be derived from Eqs. (19) and (20) as follows:
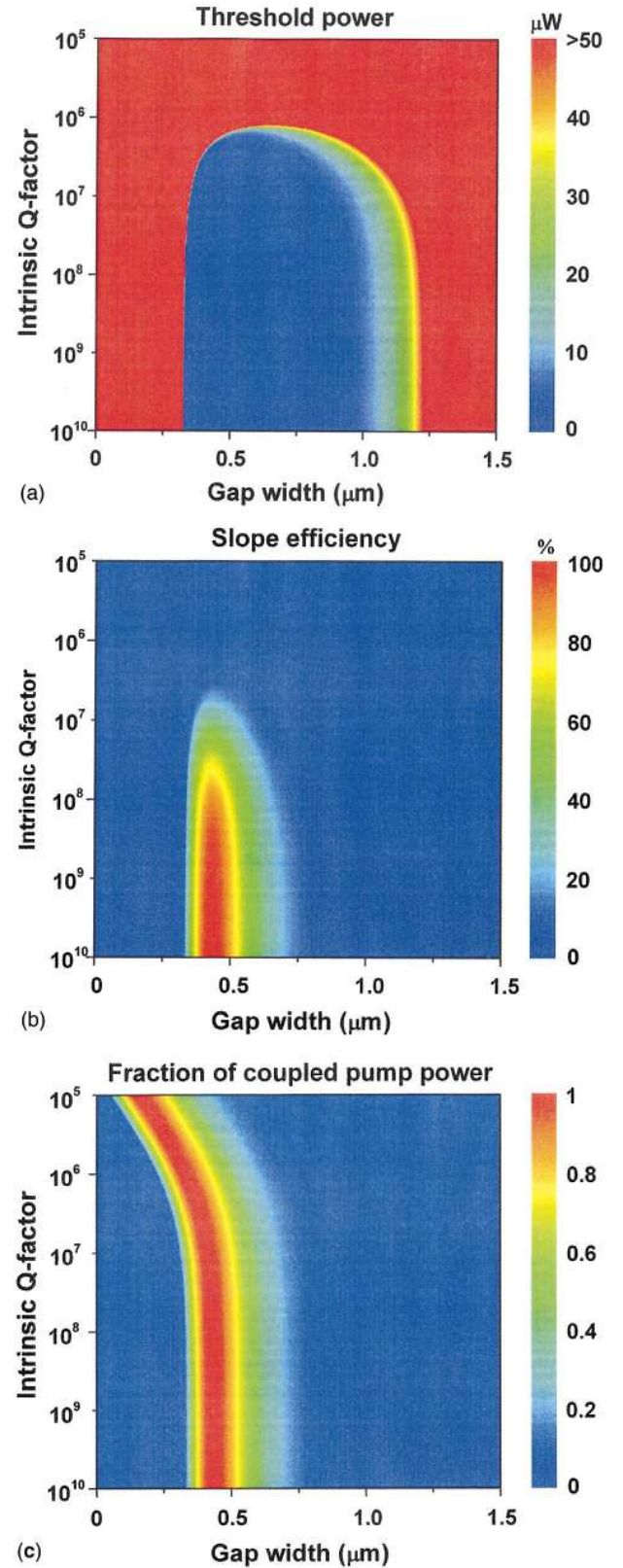

FIG. 4. (Color) (a) Threshold power; (b) slope efficiency; and (c) fraction of coupled pump power, all calculated as a function of gap width and intrinsic Q factor.

$$\eta \equiv \frac{dP_L}{d|s_p|^2}$$

$$= \kappa_s^2 \left(\frac{\nu_s n_s V_m^s}{\nu_p n_p V_m^p} \right) \frac{\alpha_p(\alpha_s + g_s^*) - (\alpha_p + g_p^*)(\alpha_s + \alpha_s^{passive})}{\alpha_s^{passive}(\alpha_s + g_s^*)}$$

$$\times \frac{4 n_p^2 \kappa_p^2 (\alpha_s + g_s^*)^2}{c^2 [(\alpha_p + \alpha_p^{passive})(\alpha_s + g_s^*) - (\alpha_p + g_p^*)(\alpha_s + \alpha_s^{passive})]^2}.$$

$$(24)$$

Figure 4 shows: (a) the input threshold power; (b) the slope efficiency; and (c) the fraction of coupled input pump power, all as a function of cavity loading (gap width) and intrinsic Q factor, calculated using (21), (24), and (22) using the same parameters as in Fig. 3. Figure 4(a) shows that at a given Q factor, the minimum threshold power is a sensitive function of gap width as also shown in Fig. 3. The threshold increases sharply in the overcoupled regime (small gap width) due to the sharp increase in cavity loss, and in the undercoupled regime due to pump-coupling inefficiency from the fiber to the resonator. For an optimum gap width, the threshold increases for decreasing intrinsic Q factor.

The slope efficiency [Fig. 4(b)] reaches ~100% for very high Q factor (10^{10}) at an optimum gap width of ~0.5 μm. It drops rapidly at over- and undercoupled conditions. This optimum gap width for the lowest threshold power and highest slope efficiency in Figs. 4(a) and 4(b) corresponds to a slightly undercoupled condition, as can be seen in Fig. 4(c). This figure also shows that the critical coupling point (as inferred by the gap width) is roughly constant for high intrinsic Q factors and moves towards the microcavity as intrinsic Q factor decreases (or $Q < 10^6$). This change of critical coupling point is caused by the variation of intrinsic erbium-related Q factor [$Q_{o,p}^{Er}$, defined in (15)]. As the intrinsic Q factor decreases below 10^7, the intrinsic erbium-related Q factor becomes independent of erbium parameters and related only to the intrinsic Q factor, leading to a decrease in critical coupling gap width.

Asymmetries of threshold power, slope efficiency, and the fraction of coupled power with respect to gap width of minimum/maximum value are observed in Fig. 4. These asymmetries result from the lasing condition imposed on minimum gap width for lasing (maximum achievable gain should be larger than the total round-trip loss), which will be discussed in the next section.

E. Lasing condition revisited

Equation (9) can be used to establish a lower bound for the erbium ion concentration required to obtain lasing in a cavity with a given passive Q factor. Taking into account that the maximum upper-state population cannot exceed the total erbium ion concentration ($N_2 < N_T$) in (9)

$$g_s^* > \alpha_s^{passive}. \qquad (25)$$

Equation (25) sets the limit on the minimum erbium concentration at fixed passive intrinsic quality factor required to overcome loss. Rewriting (25) using the constituent relation given by (8) and (10), the minimum erbium ion concentration is bounded by
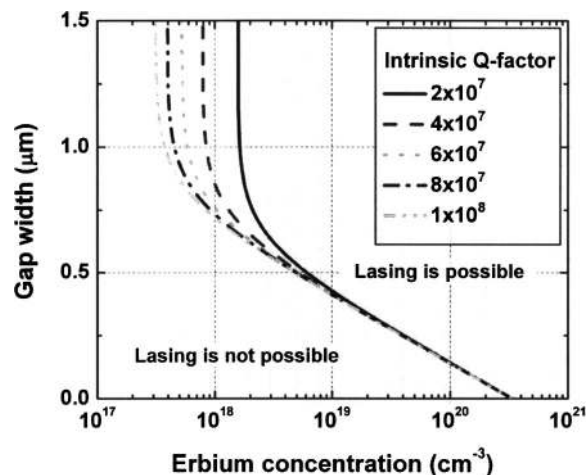

FIG. 5. Gap width to obtain lasing at a given erbium concentration. Data are shown for different passive cavity intrinsic quality factor $Q_o^{passive}$ in the range from 2×10^7 to 1×10^8.

$$N_T > \frac{2 \pi n_s}{\lambda_s \Gamma_s \sigma_s^e Q_{T,s}^{passive}}. \qquad (26)$$

As an illustrative example, by assuming the parameters discussed above and a passive Q factor of 5×10^7, the erbium concentration should be greater than 7.3×10^{17} cm^{-3} (0.001 at. %). Under 980-nm pumping nearly complete inversion is feasible and the limits contemplated in Eq. (26) may be achieved. However, when pumping occurs in the erbium absorption band at or slightly below 1.5 μm, pump-stimulated emission must be taken into account. A tighter bound on N_T is then obtained by following two lines of reasoning.

First, from (19), the following inequality is required for positive differential slope efficiency (i.e., lasing operation):

$$\alpha_p \frac{(\alpha_s + g_s^*)}{(\alpha_p + g_p^*)} - \alpha_s > \alpha_s^{passive}. \qquad (27)$$

For the special case of 980-nm band pumping (at which wavelength the emission cross section is nearly zero), Eq. (27) becomes identical to (25). However, in general (27) is a stricter condition. Inequality (27) can also be obtained by setting a limit on the maximum achievable population inversion in Eq. (9)

$$\frac{N_2}{N_T} < \frac{\alpha_p}{\alpha_p + g_p^*}, \qquad (28)$$

which is the limit of population inversion when the pump energy is high in (18) (i.e., is near the emission band).

Figure 5 is a plot of the gap width above which lasing is possible at a given erbium concentration. Curves are shown for passive cavity Q factors ranging from 2×10^7 to 1×10^8. Several features are apparent in the figure. First, for a fixed passive intrinsic Q factor, there is a minimum erbium ion concentration required for lasing action. As the passive intrinsic Q factor becomes larger, the required minimum erbium ion concentration decreases. Second, for high erbium ion concentration, the minimum gap width for lasing de-

creases and eventually becomes zero (at which point the tapered fiber and microcavity contact each other). This characteristic concentration (3.4×10^{20} cm^{-3}, 0.5 at. % in this case) above which lasing can be observed with zero gap width is independent of intrinsic Q factors and determined mainly by erbium parameters and microcavity size parameters.

F. Dependence on erbium concentration

For the purpose of optimizing the coupled threshold power and differential slope efficiency as a function of erbium ion concentration, Eqs. (21) and (24) are evaluated. In this analysis, cooperative up-conversion or ion pairing are not taken into account. Instead, to take into account concentration quenching and subsequent lifetime shortening of the erbium ions, the concentration-dependent erbium upper-state lifetime τ_{Er,N_T} is assumed to follow the reduction formula (with quenching concentration N_Q of 5×10^{20} cm^{-3} assumed) given in Ref. [32]

$$\tau_{Er,N_T} = \frac{\tau_{Er}}{1 + (N_T/N_Q)^2}. \tag{29}$$

Figure 6(a) shows the minimum achievable threshold power plotted as a function of erbium concentration and intrinsic Q factor. For a given Q factor, there is an optimal erbium ion concentration, which gives the lowest input threshold power. The higher the intrinsic Q factor, the lower the optimum erbium concentration. On either side of the optimum concentration, the threshold power increases sharply with concentration. The increase on the low-concentration side is caused by condition (27); the increase on the high-concentration side is caused by concentration quenching, increase in pump transmission [reduced pumping efficiency; see Fig. 4(c)], and higher erbium concentration itself. Figure 6(b) shows the maximum achievable differential slope efficiency as a function of total erbium ion concentration and intrinsic Q factor. At a given Q factor, the slope efficiency initially becomes larger as the erbium concentration increases, and then becomes smaller beyond a characteristic erbium concentration of 9×10^{20} cm^{-3} (~ 1.4 at. %). For a given Q factor $> 10^6$, ~ 100 % efficiency can always be achieved, provided the Q factor and junction ideality are sufficiently high. Note that while these calculations do take into account the concentration-quenching related reduction in lifetime at high erbium ion concentrations, cooperative up-conversion is not taken into account. This effect reduces the effective erbium ion population that can be achieved at a given pump power. Inclusion of this effect will cause a reduction in the achievable slope efficiency at given erbium ion concentration and Q factor.

G. Mode volume, external coupling efficiency, and size of toroidal microcavity

The expressions derived in this section can be applied to any erbium-doped laser analysis. In this paper, the laser cavity corresponds to a toroidal microcavity, and the coupling, both to and from the toroidal microcavity, is achieved by evanescent-field coupling using a tapered optical fiber
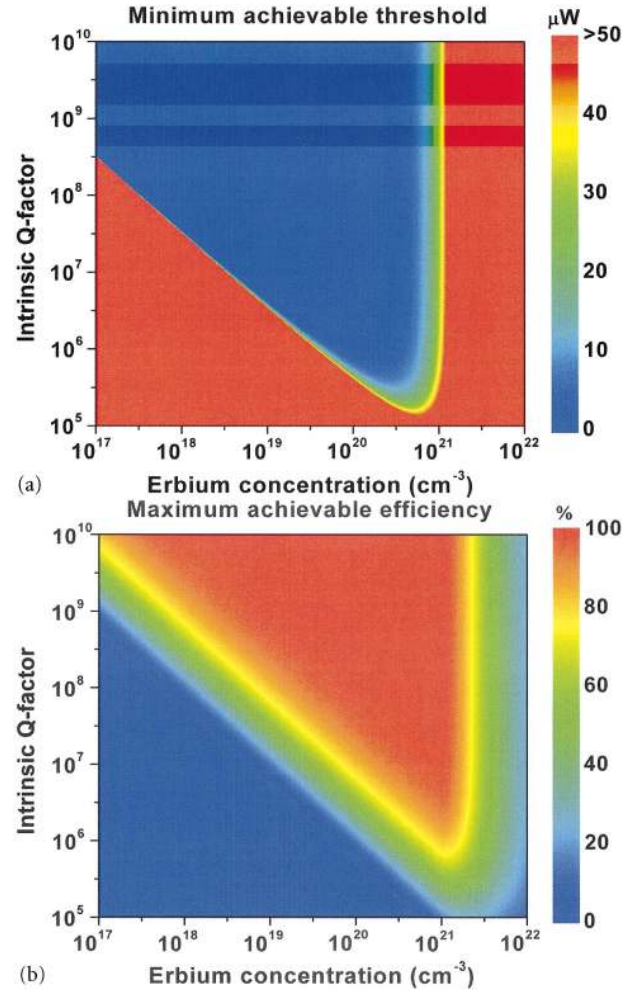

FIG. 6. (Color) (a) Minimum achievable threshold power plotted as a function of erbium ion concentration and intrinsic Q factor. (b) Maximum achievable differential slope efficiency plotted as a function of erbium concentration and intrinsic Q factor.

[22,33,34]. Because analytic expressions are not available for the coupling dependence on gap width and mode volume, the present analysis uses values in comparably sized microspheres for which there are readily available analytical expressions [20,30]. This will cause slight differences in the results. For example, the mode volume in a toroidal microcavity is smaller than that in a spherical cavity of the same diameter [35]. It is an approximately quadratic function of the major diameter of toroidal microcavity. As the lasing threshold is linear in mode volume [see Eq. (21)], the lowest lasing threshold power is expected for small toroids. For very small toroids, however, radiative (whispering-gallery) loss becomes dominant, and thus the smallest diameter of a toroidal microlaser that can be practically achieved is determined by a balance between gain (erbium concentration) and loss, given a certain available pump power. From a calculation assuming an erbium concentration of 2.5×10^{20} cm^{-3} (for which the effects of concentration quenching and cooperative up-conversion are relatively small) and the known size-dependent whispering-gallery loss [30], it follows that the smallest toroidal microcavity diameter is typically ~ 15 μm.

III. FABRICATIONS

In this section we present fabrication procedures and structural data on toroidal microlasers that were doped with erbium by ion implantation. The starting platform for the fabrication of these microcavities is an intrinsic Si(100) wafer with a 2-μm-thick SiO_2 film grown by thermal oxidation. The fabrication consists of five steps involving erbium ion implantation, high-temperature thermal annealing, photolithography, wet/dry etching, and CO_2 laser reflow/annealing.

Erbium ion implantation is performed with 2-MeV erbium ions at fluences of 1.2×10^{15}, 4.2×10^{15}, and 1.2×10^{16} cm^{-2} using a Van de Graaff accelerator. The erbium doping depth profile was measured by Rutherford backscattering spectrometry and is well fitted by a Gaussian with a peak depth of 562 nm and a standard deviation of $\sigma = 75$ nm. The peak erbium ion concentrations for the three implant fluences were 0.10, 0.35, and 1.0 at. %, respectively.

To optically activate the erbium ions, the implanted wafer was annealed at 800 °C for 1 h in vacuum. Our data demonstrate that the 800 °C thermal anneal is sufficient to restore the silica network's structure, to incorporate erbium ions on optically active sites, and to reduce the defect density to a low level so that high intrinsic Q factor is achieved (see further on). The photoluminescence lifetime at 1.53 μm for the sample implanted with 4.2×10^{15} cm^{-2}, measured after annealing, is 10 ms. This value is lower than the radiative lifetime of erbium ions in thermally grown SiO_2 (17 ms), which is ascribed to concentration quenching due to resonant energy transfer among erbium ions followed by quenching at OH^- impurity sites.

Processing of the implanted wafers into toroidal microcavities proceeds as described elsewhere [18]. Figure 1 shows the graphical rendering of the toroidal microcavity with tapered optical fiber, and the inset in Fig. 7 shows a scanning electron microscope (SEM) image of a toroidal microcavity (major diameter of 23 μm) used in the experiment. Briefly, after the high-temperature annealing process, circular photoresist pads (40–100-μm diameter) are created on the erbium-implanted silica film by standard photolithography. Next, the sample is immersed in buffered HF at room temperature to remove unpatterned silica. In this way, arrays of circular silica disks are fabricated on the silicon chip. Isolation of the silica disks from the silicon substrate is needed to prevent unwanted light leakage into the silicon substrate. This is achieved by isotropic, silicon dry etching using XeF_2, leaving silica disks supported by a silicon pillar structure.

Finally, to create ultrahigh-Q toroidal microcavities, the silica disks are selectively reflowed by irradiation using a CO_2 laser ($\lambda = 10.6$ μm). As has been demonstrated before [18], this leads to melting and subsequent collapsing of the silica disk to a toroidal shape, with limiting dimensions defined by the width of the supporting silicon pillar. Toroidal microcavities made in this way exhibit record high-Q factors for planar devices in excess of 10^8 and therefore make excellent base resonators for the study of erbium-doped laser structures [16,17].

To study the effect of laser annealing on the optical properties of the erbium ions, we measured luminescence decay traces at 1.535 μm for both disk and toroidal microcavities
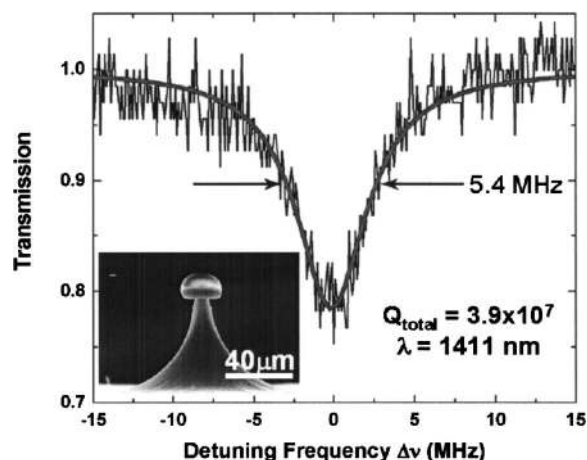

FIG. 7. High-resolution whispering-gallery mode spectrum. Inset: SEM micrograph of a microcavity used in the experiment.

(i.e., both pre- and postreflow process), and they exhibit similar lifetimes of ~10 ms [17]. In the following analysis we have assumed that as a result of the laser annealing, the erbium ions are homogeneously distributed throughout the toroidal volume, at average concentrations of 6×10^{18}, 2×10^{19}, and 6×10^{19} cm^{-3}, for the three implant fluences, respectively (corresponding to concentrations of 0.009, 0.03, and 0.09 at. %, respectively).

IV. EXPERIMENTS

A typical high-resolution transmission spectrum measured through the fiber coupled to the erbium-implanted toroidal microcavity (4.2×10^{15} erbium/cm^2) is shown in Fig. 7. The spectrum was measured by scanning a narrow-linewidth (<300 kHz), tunable (1400–1500 nm), external-cavity laser across a toroidal microcavity whispering-gallery resonance and monitoring the transmitted power using a photodetector (125 MHz). The frequency scanning speed (<100 Hz) of the laser was carefully chosen to satisfy both the quasi-steady-state condition imposed by the erbium ion decay rate and the maximum scanning speed condition required for the precise measurement of high-Q factors. To couple light efficiently in and out of the erbium-implanted toroidal microcavity, a tapered optical fiber (diameter of 1–2 μm) was aligned in the equatorial plane of the toroidal microcavity. Taper fabrication and coupling characteristics are described elsewhere [22,33,34]. The microcavity was attached to a piezoelectric stage (minimum step size of 20 nm) that allowed for its precise positioning with respect to the tapered optical fiber. In the spectrum of Fig. 7, the laser center wavelength was set to 1411 nm and the resulting loaded Q factor was 3.9×10^7. To prevent thermal broadening and spectral distortion [36] associated with the high Q, the input power was always kept below 10 μW during measurement of the resonance. Because the measurement was performed in the undercoupled regime (~79 % transmission) and well below the lasing threshold, i.e., with the major fraction of the erbium ions in the ground state $^4I_{15/2}$, the observed linewidth provides a good estimate of the unloaded Q factor. The erbium absorp-
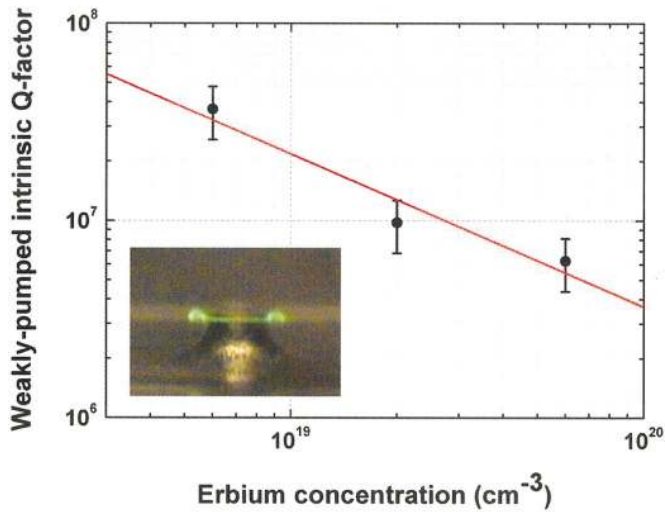
FIG. 8. (Color) Measured weakly pumped intrinsic Q factor (normalized to the pump wavelength of 1450 nm) as a function of erbium concentration and its linear fit on a log-log scale. Inset: up-conversion luminescence observed in toroidal microcavity with implantation fluence of 1.2×10^{16} cm^{-2}.

tion related contribution to Q factor can be estimated using (17) and yields $Q_{wp}^{Er} = 3.25 \times 10^7$ (assuming $N_T = 2 \times 10^{19}$ cm^{-3}, $\sigma_p^a = 1 \times 10^{-22}$ cm^2, $n_p = 1.46$, and $\Gamma_p = 1$). It is therefore believed that the measured Q factor is predominantly caused by the absorption of erbium ions.

To confirm the inverse relation between weakly pumped intrinsic Q factor and erbium ion concentration given by (16) and (17), weakly pumped Q factors at three different concentrations were measured as shown in Fig. 8. A complication that arises when comparing Q factors for different resonators is that all resonators have different resonance wavelengths, determined by their slightly different geometry. In order to compare Q factors, they have been normalized to values at a wavelength of 1450 nm, using the known erbium absorption cross-section spectrum [25] as a(n) (inverse) normalization factor. The line in Fig. 8 provides the expected inverse relation between Q factor and erbium concentration and fits the data well. This further confirms that the measured Q factors are dominated by erbium-related absorption. The inset of Fig. 8 shows a side-view color optical micrograph of a toroidal microcavity with high doping concentration (erbium ion fluence 1.2×10^{16} cm^{-2}, 0.09 at. % average), under high-intensity pumping. Green emission, resulting from second-order cooperative up-conversion between excited erbium ions, is clearly seen. This green emission was not observed for toroidal microcavities doped at lower erbium concentrations (for which data in Figs. 9–11 are shown).

Figure 9 shows the measured output lasing power versus fiber-coupled, input pump power for a microlaser implanted with 4.2×10^{15} erbium/cm^2. To pump the microlaser, the same laser used to measure the absorption spectrum in Fig. 7 was tuned to a toroidal microcavity resonance within the absorption band (1460–1480 nm) of the erbium ions. Input pump power and lasing output power were carefully measured in order to account for modest amounts of tapered fiber loss. Two sets of measurements corresponding to two differ-
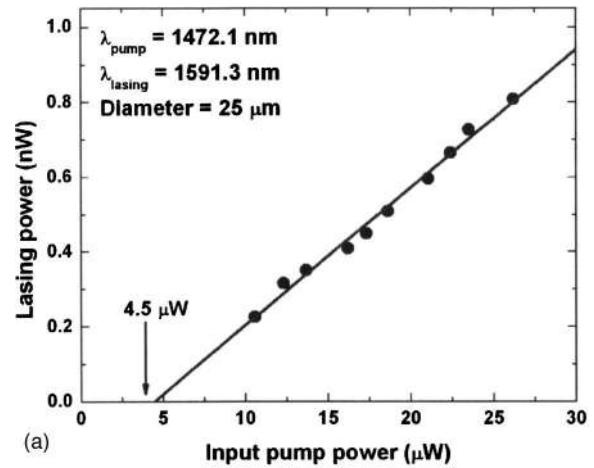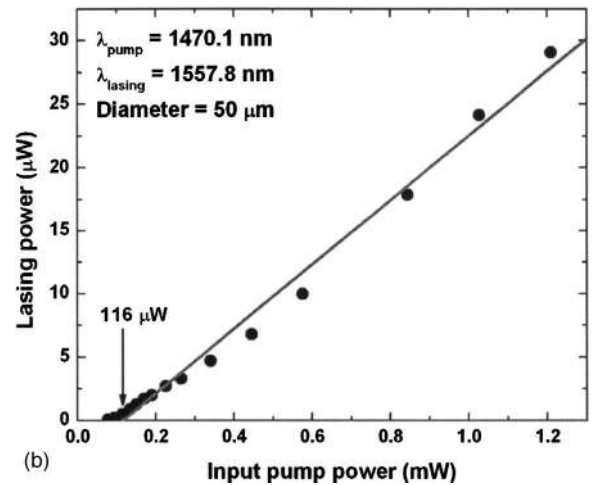
FIG. 9. Measured lasing power as a function of input pump power for two different microcavity lasers showing two distinctive regimes of operation. (All data are obtained for toroidal microcavities with a fluence of 4.2×10^{15} cm$^{\times 2}$.) (a) Low threshold fiber-launched power obtained from microcavity of 25-μm diameter. (b) High output power obtained from microcavity of 50-μm diameter.
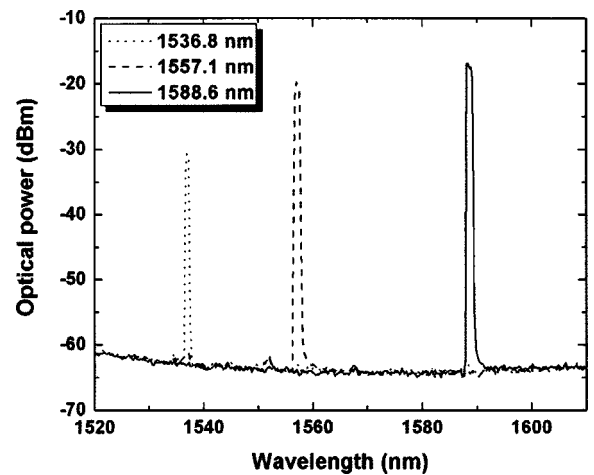

FIG. 10. Discrete lasing wavelength control by variation of the waveguide-resonator gap distance (50-μm toroidal microcavity).
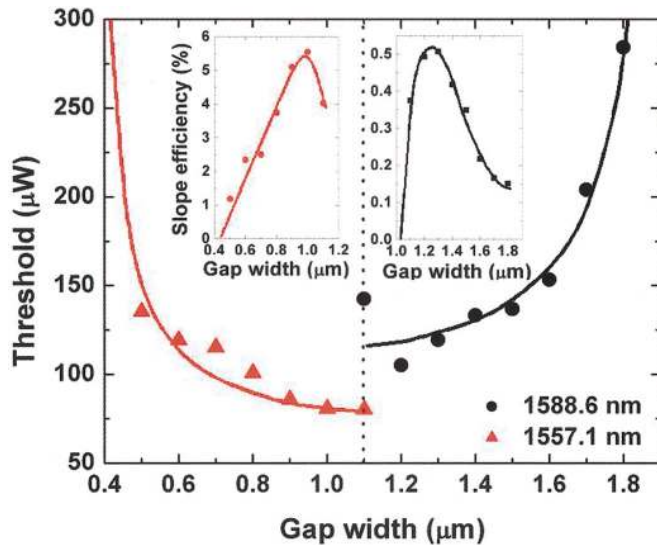
FIG. 11. (Color) Threshold power as a function of gap width between the tapered fiber and the microcavity for two sequential lasing modes. Inset: Differential (unidirectional) slope efficiency as a function of gap width between the tapered fiber and the microcavity for the same lasing modes. The lines are drawn as guides for the eyes.

ent toroidal microcavities are presented in Fig. 9. These devices illustrate two distinctive operating conditions (low threshold and high output power). The order of magnitude difference in threshold powers of these devices is attributed to the difference in the size of microcavities as well as in the Q factor. In Fig. 9(a), a threshold power of 4.5 μW is observed for a 25-μm-diameter toroidal microcavity (lasing wavelength of 1591.3 nm and pump wavelength of 1472.1 nm). The pump transmission was about ~50% in this measurement, so the actual coupled threshold pump power is estimated to be approximately 2–3 μW. This is, to the best of the authors' knowledge, the lowest threshold power reported for any erbium-doped laser. In this case, the Q factor was so high that even at very low input pump power (<100 μW), thermally induced resonance broadening [36] and associated increase in pump power transmission (due to a finite frequency scanning range in experiment) resulted in a saturated output lasing power which prohibited further output power increase.

Figure 9(b) shows a measurement with relatively high output lasing power (unidirectional slope efficiency=2.6%) measured using a 50-μm-diameter toroidal microcavity. The measured output power was 29 μW and the input threshold power was 116 μW. From a series of experiments on the same microcavity and for different cavity loading conditions, the highest (unidirectional) output power measured was 39.4 μW and the highest unidirectional slope efficiency was about 5.5 %. The dependence of threshold, slope efficiency, and lasing wavelength on cavity loading (i.e., the gap width) by the tapered fiber was also investigated. Figure 10 contains a series of lasing wavelength scans under varying loading conditions and illustrates the effect of increased cavity loading on oscillation wavelength. This measurement was performed using the same microcavity laser of Fig. 9(b). At
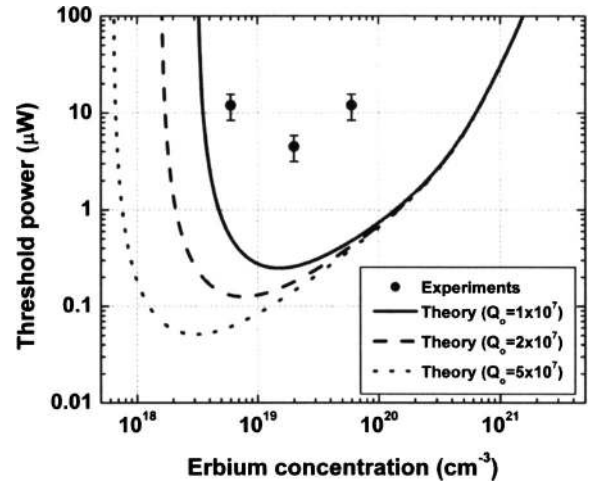

FIG. 12. Minimum threshold power achieved from different samples with various erbium concentrations. Theoretical minimum threshold powers are plotted for three different intrinsic Q factors assuming a cavity with major diameter of 50 μm.

large gap width (corresponding to the undercoupled or weakly loaded regime), lasing at relatively longer wavelengths (1588.6 nm) is observed. As the gap width decreases (cavity loading increases), the lasing wavelength shifts in discrete steps to shorter wavelengths, enabling us to broadly tune the lasing wavelength by the adjustment of cavity loading. This effect is believed to be due to the cavity-loading-induced change in the inversion of erbium ions [Eq. (9)]. In particular, as the loading increases (gap width decreases), and thus loaded Q factor decreases, the oscillation wavelength must adjust to shorter wavelengths where the available erbium gain is larger (assuming that the Q factors are the same for all the whispering-gallery modes in the erbium gain bandwidth). This kind of discrete wavelength tuning was possible only in microcavities of moderate sizes. For larger cavity diameter (>70–80 μm), and hence smaller free spectral range (FSR), multimode lasing was dominant. For smaller diameters below ~40 μm, the FSR is so large that within the erbium gain spectrum only one lasing wavelength satisfies the lasing condition, at an erbium upper-state population determined by the gap width.

The input threshold power and unidirectional slope efficiency were investigated as a function of cavity loading for two lasing wavelengths, 1557.1 and 1588.6 nm. Figure 11 shows the input threshold power as a function of gap width between the tapered fiber and the microcavity. In the undercoupled regime, lasing starts at a relatively long wavelength (1588.6 nm) first with high threshold due to the small pump coupling. As the gap width decreases, the threshold decreases at first, but ultimately increases abruptly near the gap-distance limit (~1.1 μm) defined by the condition (27). Eventually lasing at 1588.6 nm can no longer be supported because the increased cavity loading (and hence reduced Q factor) cannot be compensated by the relatively small gain at this wavelength (small emission cross section). As the coupling distance is further reduced, the next lasing line at 1557.1 nm appears and similarly, the threshold power is observed to increase near the gap-distance limit (~0.4 μm for this wavelength).

The inset in Fig. 11 shows the differential slope efficiency as a function of gap width for the two lasing wavelengths. Starting from the weakly loaded regime, the differential slope efficiency increases as the cavity loading increases and reaches a maximum, in quantitative agreement with the calculations in Fig. 4(b). The same is observed for the second lasing line that appears with increased loading. For each lasing wavelength, the lowest threshold and highest slope efficiency are achieved at the same optimum gap width, in agreement with Fig. 4.

Figure 12 shows the threshold power measured for toroidal microcavities having three different erbium concentrations. The top axis shows the erbium concentration assuming erbium ions are homogeneously distributed in the toroidal microcavity. In each case, multiple measurements were performed on a series of toroidal microcavities with the same erbium ion fluence, and the lowest measured threshold was plotted in Fig. 12. The data show only a weak dependence on erbium concentration. This, and the absolute values of the measured thresholds, is in qualitative agreement with Fig. 6, which shows a weak dependence on concentration in the concentration range 7×10^{18}–3×10^{19} cm^3 for an intrinsic Q of 10^7, typical for our experiments.

V. CONCLUSIONS

Lasing in erbium-implanted high-Q silica microcavities coupled to a tapered fiber has been investigated analytically and experimentally. Threshold powers as low as 4.5 μW and output power of 39.4 μW are experimentally achieved using differently sized resonators and coupling conditions. Controlling the lasing wavelength was possible by changing the tapered-fiber-microcavity gap width. Formulas predicting various performance metrics such as threshold power, differential slope efficiency, optimum concentration of erbium ions, as well as the influence of resonator size and the Q factors were derived and the calculations are in good agreement with the experimentally obtained results.

[1] M. L. Gorodetsky, A. A. Savchenkov, and V. S. Ilchenko, Opt. Lett. **21**, 453 (1996).

[2] D. W. Vernooy, V. S. Ilchenko, H. Mabuchi, E. W. Streed, and H. J. Kimble, Opt. Lett. **23**, 247 (1998).

[3] J. B. Snow, S.-X. Qian, and R. K. Chang, Opt. Lett. **10**, 37 (1985).

[4] S.-X. Qian and R. K. Chang, Phys. Rev. Lett. **56**, 926 (1986).

[5] A. J. Campillo, J. D. Eversole, and H.-B. Lin, Phys. Rev. Lett. **67**, 437 (1991).

[6] H.-B. Lin and A. J. Campillo, Phys. Rev. Lett. **73**, 2440 (1994).

[7] S. Arnold, M. Khoshsima, I. Teraoka, S. Holler, and F. Vollmer, Opt. Lett. **28**, 272 (2003).

[8] V. Sandoghdar, F. Treussart, J. Hare, V. Lefèvre-Seguin, J.-M. Raimond, and S. Haroche, Phys. Rev. A **54**, R1777 (1996).

[9] K. Sasagawa, K. Kusawake, J. Ohta, and M. Nunoshita, Electron. Lett. **38**, 1355 (2002).

[10] W. von Klitzing, E. Jahier, R. Long, F. Lissillour, V. Lefevre-Seguin, J. Hare, J.-M. Raimond, and S. Haroche, Electron. Lett. **35**, 1745 (1999).

[11] L. Yang and K. J. Vahala, Opt. Lett. **28**, 592 (2003).

[12] X. Peng, F. Song, S. Jiang, N. Peyghambarian, and M. Kuwata-Gonokami, Appl. Phys. Lett. **82**, 1497 (2003).

[13] M. Cai, O. Painter, K. J. Vahala, and P. C. Sercel, Opt. Lett. **25**, 1430 (2000).

[14] F. Lissillour, D. Messager, G. Stéphan, and P. Féron, Opt. Lett. **26**, 1051 (2001).

[15] M. Cai and K. Vahala, Opt. Lett. **26**, 884 (2001).

[16] L. Yang, D. K. Armani, and K. J. Vahala, Appl. Phys. Lett. **83**, 825 (2003).

[17] A. Polman, B. Min, J. Kalkman, T. Kippenberg, and K. Vahala, Appl. Phys. Lett. **84**, 1037 (2004).

[18] D. K. Armani, T. J. Kippenberg, S. M. Spillane, and K. J. Vahala, Nature (London) **421**, 925 (2003).

[19] H. A. Haus, *Waves and Fields in Optoelectronics* (Prentice-Hall, Englewood Cliffs, NJ, 1984), Chap. 7.

[20] M. L. Gorodetsky and V. S. Ilchenko, J. Opt. Soc. Am. B **16**, 147 (1999).

[21] M. L. Gorodetsky, A. D. Pryamikov, and V. S. Ilchenko, J. Opt. Soc. Am. B **17**, 1051 (2000).

[22] S. M. Spillane, T. J. Kippenberg, O. J. Painter, and K. J. Vahala, Phys. Rev. Lett. **91**, 043902 (2003).

[23] B. Min, T. J. Kippenberg, and K. J. Vahala, Opt. Lett. **28**, 1507 (2003).

[24] E. Desurvire, *Erbium-Doped Fiber Amplifiers: Principles and Applications* (Wiley, New York, 1994).

[25] P. C. Becker, N. A. Olsson, and J. R. Simpson, *Erbium-Doped Fiber Amplifiers: Fundamentals and Technology* (Academic Press, San Diego, 1997).

[26] P. F. Wysocki, J. L. Wagener, M. J. Digonnet, and H. J. Shaw, in Proceedings of SPIE on Fiber Laser Sources and Amplifiers IV, 1993, edited by M. J. Digonnet and E. Snitzer, 1789, p. 66 (unpublished).

[27] T. J. Kippenberg, S. M. Spillane, and K. J. Vahala, Opt. Lett. **27**, 1669 (2002).

[28] C. R. Giles and E. Desurvire, J. Lightwave Technol. **9**, 271 (1991).

[29] Y. Sun, J. L. Zyskind, and A. K. Srivastava, IEEE J. Sel. Top. Quantum Electron. **3**, 991 (1997).

[30] B. E. Little, J.-P. Laine, and H. A. Haus, J. Lightwave Technol. **17**, 704 (1999).

[31] M. L. Brongersma, E. Snoeks, T. van Dillen, and A. Polman, J. Appl. Phys. **88**, 59 (2000).

[32] W. J. Miniscalco, J. Lightwave Technol. **9**, 234 (1991).

[33] M. Cai, O. Painter, and K. J. Vahala, Phys. Rev. Lett. **85**, 74 (2000).

[34] J. C. Knight, G. Cheung, F. Jacques, and T. A. Birks, Opt. Lett. **22**, 1129 (1997).

[35] S. M. Spillane, T. J. Kippenberg, and K. J. Vahala (unpublished); B. Min, S. M. Spillane, and K. J. Vahala (unpublished).

[36] V. S. Il'chenko and M. L. Gorodetskii, Laser Phys. **2**, 1004 (1992).